ARTICLE | Article in Press

Structural characterisation of *Burkholderia pseudomallei* BPSL0610 reveals its thioesterase features

Pravin Kumran Nyanasegran · Jia Rong Tey · Anis Nadyra Zifruddin · JiaXian Ong · Sheila Nathan · Glyn R. Hemsworth · Mohd Firdaus-Raih · Nor Azlan Nor Muhammad · Chyan Leong Ng

Received: 21 August 2025 / Accepted: 17 September 2026
© The Author(s) 2026

Abstract

Burkholderia pseudomallei (BP) is the aetiological agent of melioidosis with infections resulting in significant mortality in both animals and humans. BP is known to form biofilm which has been associated with relapse in melioidosis patients. Biofilms are an aggregation of microbial cells enclosed within a self-produced extracellular polymeric matrix. The *bpsl0610* transcript was highly expressed during BP biofilm formation and the gene is present within a gene cluster (*becA-R*) that encodes the molecular machinery to produce exopolysaccharides. The BPSL0610 protein has thus been implicated in BP biofilm exopolysaccharide production. Since the specific function of BPSL0610 is unclear based on genome annotations, computational tools were utilised to determine the protein's function. The three-dimensional structure of BPSL0610 was predicted using AlphaFold2 which revealed that the protein consists of two sequential canonical α/β hydrolase domains. Both domains resemble carboxylesterases (EC3.1.1.1) but only the C-terminal domain retained a conserved catalytic triad composed of Cys_{445}, $His_{604,}$ and Asp_{571}. This suggests that the cysteine may serve as a key catalytic residue in this enzyme, a feature commonly found in thioesterases. Esterase assays of the recombinant protein of BPSL0610 was indeed displayed catalytical activity towards short chain ester substrates. Furthermore, the high confidence ternary complex structure of BPSL0610-BPSL0615 with the 4'-phosphopantetheine (4'-PP) arm on the acyl carrier protein (ACP) (BPSL0615) was predicted. The 4'-PP was shown to be positioned in in the active site of BPSL0610 with similar orientation like other reported ternary complex structures of thioesterase and carrier protein with 4'-PP attached. This suggests that hydrolysis of the thioester bond of 4'-PP bound substrate may take place in the active site of BPSL0610. Taken together, the findings suggest that BPSL0610 is likely a thioesterase, which may function as part of the proposed molecular machinery that mediates exopolysaccharide synthesis and modification in BP.

Keywords Melioidosis · Biofilms · α/β hydrolase · Thioesterase · Exopolysaccharides

This Article in Press is shared early to give you faster access to new research. It is citable and carries a permanent DOI. The final edited version will replace it automatically.

Introduction

Burkholderia pseudomallei (BP) is a Gram-negative environmental bacterium predominantly found in soil and surface water in endemic tropical and subtropical locations worldwide[1,2]. BP is the aetiological agent of melioidosis, a life-threatening disease that is predicted to result in approximately 89,000 deaths per year globally[2,3]. Melioidosis patients are known to relapse at high rates following antibiotics therapy and one reason for this is the ability of BP to form biofilms[4]. Biofilms are formed when cells become embedded in an extracellular polymeric matrix (EPS), the major components of which are polysaccharides, proteins, nucleic acids (DNA), lipopolysaccharides (LPS), and water[5–9]. The matrix serves as a barrier to resist the entry of antibiotics into the bacterial cells.

Recent studies on BP biofilms have successfully identified and characterised signalling molecules and EPS components[10–13], while omics studies have also identified several genes and proteins involved in biofilm formation by BP [10]. Comparative transcriptome analysis between BP strains with high and reduced ability to form biofilms identified 563 differentially regulated genes, indicating significant changes in gene expression during BP biofilm formation[10]. Within this set, some of the genes from a gene cluster known as *becA-R* (*bpsl0603-bpsl0620*) were seen to be upregulated during BP biofilm formation[11]. Genome scale analysis has also implicated this gene cluster is essential towards the production of exopolysaccharides in BP biofilms, since mutation of these genes leads to decreased biofilm formation. However, the precise roles of the proteins encoded by the *becA-R* cluster in BP exopolysaccharide development is yet to be determined[11].

A gene in the *becA-R* cluster, *bpsl0610*, was of particular interest as it has previously been annotated as encoding a hypothetical protein[10,14]. However, more recently, sequence similarity network (SSN) and genome neighbourhood analyses annotated BPSL0610 as an α/β hydrolase, but its function remains unknown[15]. The *bpsl0610* gene is located adjacent to the *bpsl0611-bpsl0615* cassette, a sub-set of genes within the *becA-R* gene cluster that have been termed the amino acid (acyl carrier protein, ACP) ligase (AAL) cassette[14,15]. The five proteins encoded by this cassette were annotated as glycosyl hydrolase family 2 (BPSL0611), cysteine peptidase/acyltransferase superfamily (BPSL0612), amino acid (acyl carrier protein) ligase (AAL) (BPSL0613), acyl-CoA dehydrogenase (Acd) (BPSL0614) and acyl carrier protein (ACP) (BPSL0615)[15]. These proteins encoded by the AAL cassette are predicted to be involved in the modification of surface polysaccharides in pathogenic Burkholderia through an ACP-dependent mechanism that shares functional similarities with polyketide synthases (PKSs) and non-ribosomal peptides synthetases (NRPSs)[15,16](Fig. 1). Although *bpsl0610* is not classified as part of the AAL cassette, similar α/β hydrolase annotated genes are commonly found in the *becA-R* gene cluster throughout the Burkholderiales, suggesting that BPSL0610 may function in conjunction with the AAL cassette encoded genes.

The α/β hydrolases are a large group of structurally related enzymes with diverse catalytic functions. Enzymes classified in this family include lipases, thioesterases, serine carboxypeptidases and acetylcholinesterases[17]. Some enzymes within these classes have been implicated in biofilm regulation. For example, the α/β hydrolase protein, AidH from *Ochrobactrum* sp. strain T63 reduces biofilm formation by hydrolysing the ester bond in *N*-Acylhomoserine lactones (AHLs), quorum sensing molecules that are essential for the formation of biofilms[18,19]. PgaB from *Bordetella bronchiseptica* and *Escherichia coli* also contains an α/β hydrolase domain but acts as a carbohydrate esterase (CE4) and was reported to regulate the modification of the exopolysaccharide Poly-β-1,6-*N*-acetyl-D-glucosamine (PNAG) through a metal-dependent deacetylation reaction, essential for biofilm formation in these species[20–22]. The autotransporter esterase, EstA of *Pseudomonas aeruginosa* was reported to produce rhamnolipids that are crucial for cell motility and biofilm formation[23]. In addition, a putative lipase, BipL in the same species was also reported to suppress biofilm formation by altering the composition of the biofilm matrix[24]. Thioesterases (TEs) in the α/β hydrolase class have also demonstrated functions in microbial biofilm regulation. For instance, Bcam0581 that displays TE activity in *Burkholderia cenocepacia* releases *cis*-2-dodecenoic acid (BDSF) following synthesis by hydrolysing the thioester bond that links the BDSF molecule and ACP on which it was assembled[25]. BDSF is a quorum sensing signalling molecule that has been shown to regulate virulence and biofilm formation in *B. cenocepacia*[25]. The diverse functions and roles of α/β hydrolases in biofilm formation,

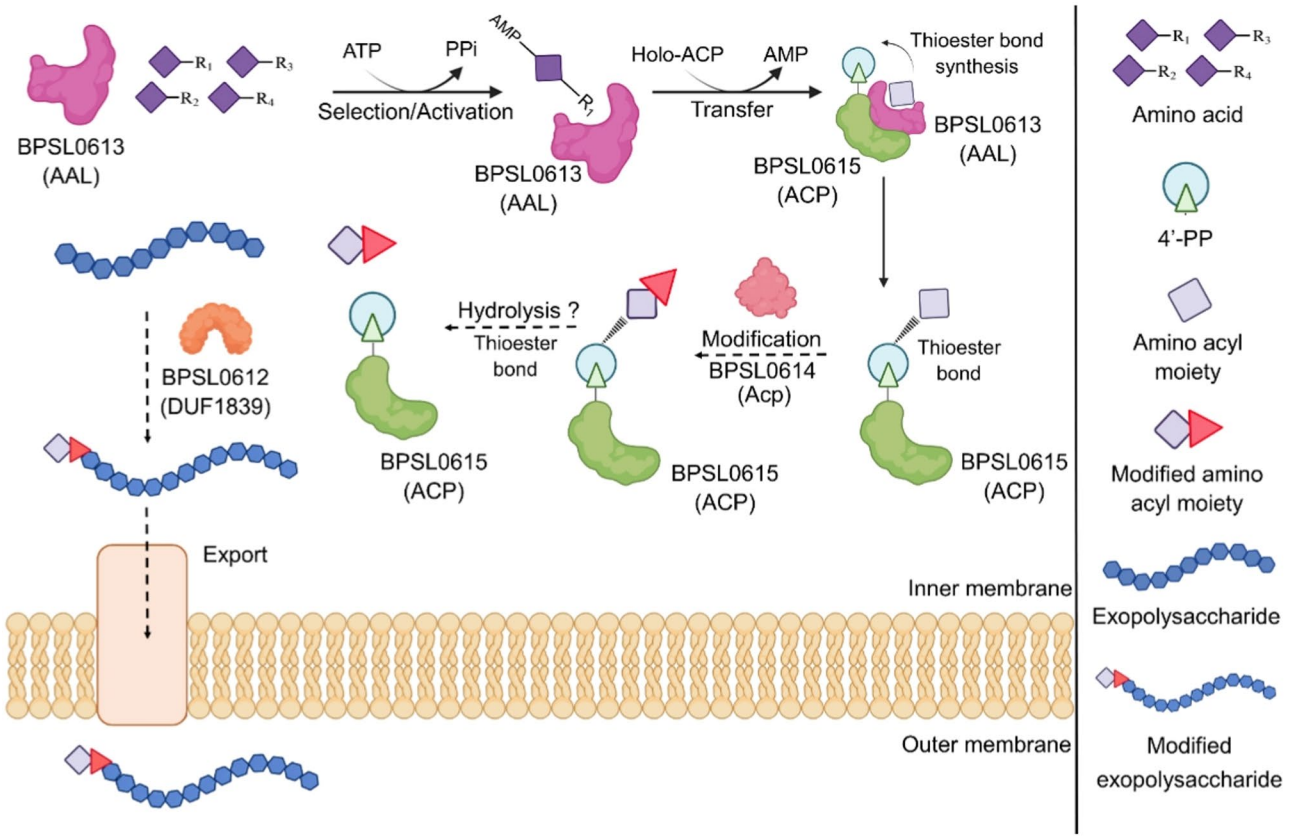


Fig. 1 Proposed exopolysaccharide modification pathway. Based on Simunović et al[15], the amino acid (acyl carrier protein) ligase (AAL), BPSL0613 activates an amino acid by forming an aminoacyl-AMP intermediate from ATP. The aminoacyl moiety is subsequently transferred to the 4'-phosphopantetheine arm (4'-PP) on the acyl carrier protein (ACP), BPSL0615 via a thiolation reaction, resulting in the formation of a thioester bond. It is then proposed that the amino acyl moiety is modified by a putative acyl-CoA dehydrogenase, BPSL0614 before being transferred onto the exopolysaccharide. The molecular machinery that is responsible for this transfer is unclear. Nonetheless, the putative cysteine peptidase/acyltransferase family protein (BPSL0612) that belong to the DUF1839 protein family was hypothesised to mediate the transfer. However, the protein that facilitates the release of acyl amino moiety that is bound to the 4'-PP on the ACP has not been reported. The dotted arrows correspond to undefined mechanisms.

and the localisation of *bpsl0610* adjacent to the AAL cassette are suggestive of a new function within this class. Hence, we employed extensive computational analysis and molecular simulations to investigate the function of BPSL0610 and establish its potential role in exopolysaccharide production by BP.

Materials and methods

Sequence alignment/phylogenetics analysis

The protein sequence of BPSL0610 was retrieved from the National Centre for Biotechnology Information (NCBI) protein database (accession: CAH34603). The BPSL0610 amino acid sequence was used as a query to identify evolutionarily related sequences through the Blastp search engine in conjunction with the RefSeq Select Protein (refseq_select) database[26]. All the identified protein sequences were subjected to multiple sequence alignment using ClustalW[27]. The aligned sequences were used in the construction of a phylogenetic tree using MEGA11[28].The evolutionary history was inferred using the Maximal Likelihood (ML) statistical method and

the Le and Gascuel (LG) substitution model[29]. A total of 1000 bootstrap re-sampling was performed during the construction of the phylogenetic tree. The corresponding phylogenetic tree was visualised using Interactive Tree of Life v 6.8.1[30]. Conserved domains within the BPSL0610 amino acid sequence were identified using InterPro[31]. To assess the divergence of phylogenetic relationships between the domains identified from InterPro, independent phylogenetic analyses were performed for the predicted N-terminal (Asp_7 – Leu_{200}) and C-terminal (Val_{338} – Arg_{629}) regions of BPSL0610 using the same alignment and reconstruction procedures described above.

In silico 3D structure prediction, fold topology, and quality evaluation of the predicted structure

The three-dimensional (3D) structure of BPSL0610 was predicted using AlphaFold2 Google Collab notebook (AlphaFold2.ipynb)[32,33]. The relaxation option was enabled during generation of the predicted model. AlphaFold2 generated a total of five models and structures with high confidence were determined based on the predicted local-distance difference test (pLDDT) score and the predicted alignment error score (PAE). Ramachandran plot statistics were used to determine the stereochemical quality of the predicted models via the MolProbity structural assessment tool (http://molprobity.biochem.duke.edu/)[34]. UCSF Chimera X[35] was utilised to visualise the Alpha Fold2 structure of BPSL0610 while the fold topology of the model was analysed with PDBsum (https://www.ebi.ac.uk/thornton-srv/databases/pdbsum/Generate.html)[36].

Structure comparison and binding site prediction

The structure generated from AlphaFold2 with the highest confidence was analysed with the DALI server (http://ekhidna2.biocenter.helsinki.fi/dali/), to identify proteins with a similar 3D structure in the Protein Databank (PDB)[37]. Structures with higher similarities were determined based on the Z-score from the DALI server and the cα root mean square deviation (RMSD) from the superimposition of the structures and BPSL0610 using Chimera X [35]. Sequence alignments between the identified structural homologues with BPSL0610 were produced using T-COFFEE[38] and subsequently visualised using ESPript 3.0 (https://espript.ibcp.fr/ESPript/ESPript/)[39]. The pyKFinder module which is implemented in Chimera X was used to identify pockets and cavities on the protein surface[40].

Structure prediction of BPSL0610-BPSL0615-4′-phosphopantetheine (4′-PP) ternary complexes

The biomolecular ternary complex structure consisting of BPSL0610, BPSL0615 and 4'-PP was modelled using two different web servers, Protenix-v1, a fully open-source biomolecular structure prediction model[41], and RoseTTAFold3 (https://neurosnap.ai/service/RoseTTAFold3)[42]. The amino acid sequences of BPSL0610, BPSL0615 and the SMILES string of 4'-PP were uploaded into the Protenix and RoseTTAFold3 servers. The confidence of the model complex generated were evaluated based on pLDDT, PAE, predicted template modelling score (pTM) and the interface predicted template modelling score (iPTM).

Molecular dynamics simulation

Molecular dynamics (MD) was used to analyse the stability of the AlphaFold2 predicted model structure and the interdomain contacts between the identified N-terminal and C-terminal domains of BPSL0610. The MD simulations were also utilised to analyse the stability of ligand binding interaction of the predicted ternary complex structure. MD was performed using the Groningen Machine for Chemical Simulations (GROMACS) software v 2023.3[43]. All simulation files were generated using the CHARMM-GUI web server (https://www.charmm-gui.org/) [44]. The ligand topologies were generated using CHARMM-GUI ligand reader and modeler[45]. The protein-ligand complex from the docking was treated with CHARMM-36 force field[46] and the system was set in a cubical box with a 15 Å distance from each edge of the solvated box. The system was solvated using a transferable

intermolecular potential water molecules (TIP3P) model[47]. System neutralisation was achieved by adding sodium chloride ions with a physiological concentration of 0.15 M. The system was subjected to energy minimisation using the steepest descent algorithm up to 10,000 steps. The MD simulation consisted of two stages: system equilibration and production. The equilibration phase was performed using NVT ensemble for 125ps. Meanwhile, the production step was carried out for 100 ns at a constant temperature of 30 °C. The stability of the protein-ligand complexes throughout the simulation was analysed through the calculation of RMSD that measures the deviation of the protein backbone from its initial conformation throughout the simulation. The RMSD for the entire trajectory was calculated using the gmx rms program. Variations in the amino acid residues within the BPSL0610 structure were analysed by root mean square fluctuation (RMSF) using the gmx rmsf program[52].

Cloning and expression of recombinant BPSL0610

The nucleotide sequence of *bpsl0610* which encodes the protein BPSL0610 (Uniprot 63XC6) was ligated into the pMAL-c6T vector and transformed into the expression host *E. coli* Lemo21 (DE3). This construct produces a recombinant protein fused to a maltose binding protein (MBP) and a histidine tag located at the N-terminus region of BPSL0610 (rBPSL0610^{MBP}) (**Supplementary Fig. 1**). Briefly, five single colonies corresponding to positive transformants of *E. coli* Lemo21 (DE3) containing the plasmid pMAL-c6T-*bpsl0610* were selected and inoculated into LB media containing 120 µg/mL of ampicillin and 35 µg/mL of chloramphenicol. The culture was incubated for 16 h at 37 °C and 200 rpm. Overnight cultures were transferred into a baffled flask containing 250 mL of the same medium. The volume of the overnight culture added corresponded to a final optical density (OD_{600}) reading of ~0.02. The culture containing the corresponding antibiotics and 0.5% (w/v) glucose was incubated at 37 °C and 200 rpm until an OD_{600} of ~0.7-1.0 was achieved. The bacterial culture was then induced with isopropyl β-d-1-thiogalactopyranoside (IPTG) at a final concentration of 0.5 mM and 1% (v/v) of tween 20. The cells were cultured for 16 h at 16 °C and 200 rpm. The overexpressed culture was centrifuged (10000 x *g*, 10 min, 4 °C) and the cells were stored at -80 °C.

Purification of rBPSL0610^{MBP}

The rBPSL0610^{MBP} was subjected to a three-step purification strategy consisting of HisTrap immobilised metal ion affinity chromatography (IMAC), size exclusion (SEC) purification and MBP trap purification. Every 1 g/L of rBPSL0610^{MBP}-expressing cells were resuspended with 10 mL of binding buffer (50 mM Tris-HCl (pH 8), 1 M NaCl, 10% (v/v) glycerol, 0.2% (v/v) tween 20, 5 mM β-ME and 20 mM imidazole). The cells were lysed by sonication with 35% amplitude using five cycles of 15 s on and 30 s off pulses. The lysate was centrifuged at 10,000 x *g*, for 15 min at 4 °C. The supernatant was applied onto a prepacked HisTrap™ column containing 5 mL of Ni-NTA -Sepharose (GE Healthcare, USA) equilibrated in binding buffer at a flow rate of 1 mL/min. After sample application, the column was washed with 25 mL binding buffer prior to eluting in a gradient elution using an elution buffer (50 mM Tris-HCl (pH 8), 1 M NaCl, 10% (v/v) glycerol, 0.2% (v/v) tween 20, 5 mM β-ME and 250 mM imidazole). Fractions containing the protein of interest were identified by 15% (w/v) SDS-PAGE and subsequently pooled and concentrated using a Vivaspin concentrator fitted with a 30 kDa molecular weight cutoff filter (Sartorius, Germany). The concentrated BPSL0610^{MBP} was subjected to SEC purification using a HiLoad 16/600 Superdex 200 pg column (GE Healthcare, USA). The column was pre-equilibrated with 50 mM Tris-HCl pH 8.0, 1 M NaCl, 0.2% (v/v) tween 20, 10% (v/v) glycerol and 5 mM β-ME prior to elution at a flow rate of 1 mL/min. The purity of the purified protein was determined by 15% (w/v) SDS-PAGE. The eluate containing rBPSL0610^{MBP} protein was further purified through MBP affinity purification using a 5 mL MBP Trap HP column (GE Healthcare, USA) prepacked with Dextrin Sepharose resin. Fractions containing rBPSL0610^{MBP} from SEC were diluted with binding buffer (50 mM Tris-HCl (pH 8), 1 M NaCl, 5% (v/v) glycerol and 5 mM β-ME) to reduce the concentration of glycerol to 5% (v/v) and tween-20 to ~0.02% (v/v). The sample was applied to the MBP Trap column pre-equilibrated with binding buffer at a flow rate of 0.05 mL/min. Prior to a stepwise elution

using an elution buffer (50 mM Tris-HCl (pH 8), 1 M NaCl, 5% (v/v) glycerol, 5 mM β-ME and 100 mM maltose), the column was washed with 25 mL of binding buffer at a flow rate of 0.5 mL/min. Protein concentration was determined with the Bradford assay (Bio-RAD, USA).

LC-MS/MS identification of rBPSL0610

The purified fractions from the MBP Trap chromatography that may contain rBPSL0610^{MBP}, was subjected to peptide identification using liquid chromatography with tandem mass spectrometry (LC-MS/MS). Approximately 50 µg of rBPSL0610^{MBP} was enzymatically digested with two units of trypsin. The peptides were separated using a Vanquish Neo liquid chromatography system coupled to an Orbitrap Exploris 240 mass spectrometer. Chromatographic separation was performed with an analytical column of 75 µm × 25 cm and a trap column of 300 µm × 0.5 cm. Peptides were eluted using solvent A (water) and solvent B (80% (v/v) acetonitrile) over a 60-min gradient. The gradient was initiated at 4% solvent B, increased to 4.5% at 0.7 min and 5% at 1 min, followed by an increase to 20% at 36 min and 35% at 53 min. The column was subsequently washed by increasing solvent B to 55% at 54 min and 99% from 54.8 to 58.8 min, before re-equilibration to 4% solvent B at 60 min. The flow rate was maintained at 0.30 µL/min during peptide separation. Mass spectrometry was operated in positive ion mode with, full MS scans were collected in the mass range of 350–1200 m/z. The identified peptide sequences were then searched against the BP proteome (UP000000605) and *E. coli* proteome (UP000000625) using MaxQuant[48].

Esterase activity assay

Enzyme activity was measured spectrophotometrically using the *p*-nitrophenyl (*p*NP) esters acetate (C2), butyrate (C4), caproate (C6) and decanoate (C10). All substrates were dissolved in 100% (v/v) acetonitrile to a concentration of 10 mM. The standard reaction system was carried out for 10 min at 37 °C in 1.425 mL of 50 mM Tris-HCl buffer (pH 8), 15 µL of 10 mM *p*NP substrates, 60 µL of 100% (v/v) acetonitrile. The reaction was initiated by the addition of 20 µL of protein (0.08 mg/mL). Several controls were included in the esterase activity assay. The negative controls were lysate of *E. coli* Lemo21 DE3 which was grown at OD_{600} ~2.5 nm and purified MBP protein ~ 43 kDa. Porcine pancreatic lipase ~ 50 kDa (Sigma Aldrich, USA) was used as a positive control. The release of *p*-nitrophenol was determined spectrophotometrically at 410 nm (PerkinElmer LAMBDA 365 + UV/Vis, UK). One unit of enzyme is defined as the amount of enzyme releasing 1 µmol of *p*-nitrophenol per minute. The molar extinction coefficient value of *p*NP at OD_{410} is 17,800 $M^{-1}cm^{-1}$ [49]. The substrate exhibiting the highest enzymatic activity was defined as 100% relative activity and the relative activity of other substrates were compared to the substrate exhibiting the highest enzymatic activity. The relative activity is presented as the mean ± standard error of three independent measurements for each substrate. The kinetic parameters of rBPSL0610^{MBP} were determined using a constant enzyme concentration of 0.5 mg/mL and substrate concentration range of 14–20 mM. The K_M and V_{max} values were determined from the Lineweaver-Burk plot while catalytic efficiency of rBPSL0610^{MBP} was expressed as k_{cat}/K_M. The value was calculated by using the values of K_M, V_{max} and the molecular weight of rBPSL0610^{MBP}. The values of the kinetic parameters are presented as the mean ± standard error of three independent measurements.

Results

Sequence alignment/phylogenetic analysis

The coding sequence of *bpsl0610* contains 658 amino acids and the ProtParam Expasy tool indicated that BPSL0610 has an estimated molecular weight of 73.3 kDa and isoelectric point of 9.22. The protein was annotated as a hypothetical protein in the NCBI protein database (GenBank: CAH34603.1) and The Burkholderia Genome Database

(https://www.burkholderia.com/) [14]. However, blastp analysis showed that BPSL0610 shares ~ 35% sequence identity to proteins annotated as alpha/beta (α/β) hydrolases. Phylogenetic analysis revealed that BPSL0610 and its orthologs are widely distributed across prokaryotes, including Pseudomonadota/Proteobacteria, Planctomycetes, Verrucomicrobia and Chlamydiae (PVC), Actinomycetes, Bacteroidetes, Thermodesulfobacteriota, and Myxococcota (Fig. 2). BPSL0610 is highly conserved under the phylum of Pseudomonadota which is one of the largest phyla within the bacterial domain[50]. The analysis of the domain organisation using InterPro further revealed that BPSL0610 consists of two α/β hydrolase domains located at the N-terminal (Asp_7 – Leu_{200}) and C-terminal (Val_{338} – Arg_{629}). The evolutionary relationship between both identified α/β hydrolase domains were also evaluated independently (**Supplementary Fig. 2A-B**). The similar phylogenetic topology observed suggests that both domains may have evolved in parallel. Given the link to a potential role of BPSL0610 in biofilm formation, the species that were identified in the phylogenetic tree were also analysed through a literature search for their ability to form biofilm. Nonetheless, only *Burkholderia mallei* were reported to form biofilms. This finding reveals that the biofilm-forming capacity of the remaining species remains largely uncharacterised thereby, suggesting the need for future studies to investigate biofilm formation in the analysed species that contain BPSL0610 orthologs within the class β-proteobacteria of the phylum Pseudomonadota.

Three-dimensional (3D) structure of BPSL0610

The structure of BPSL0610 was predicted using the AlphaFold2 server The five predicted models of BPSL0610 recorded pLDDT scores ranging from 82 to 82.5, revealing that the structures were predicted with high confidence. The highest-ranked AlphaFold2 model (pLDDT = 82.5) was predicted with high confidence to form two domains (Fig. 3A-C). The regions that correspond to the high pLDDT score consist of eight parallel β-sheets (β_1, β_3, β_4, β_5, β_6, β_7, β_8, β_9) and two antiparallel β sheets (β_2, β_{10}), surrounded by α helices (α_2-α_{12}) at the N terminus of the structure. The C terminal domain is similarly formed from eight parallel β strands (β_{11}, β_{11}, β_{12}, β_{13}, β_{14}, β_{15}, β_{16}, β_{18}) and two antiparallel strands (β_{17}, β_{19}), surrounded by α helices (α_{15}-α_{24}). (Fig. 3C). The PAE score, which

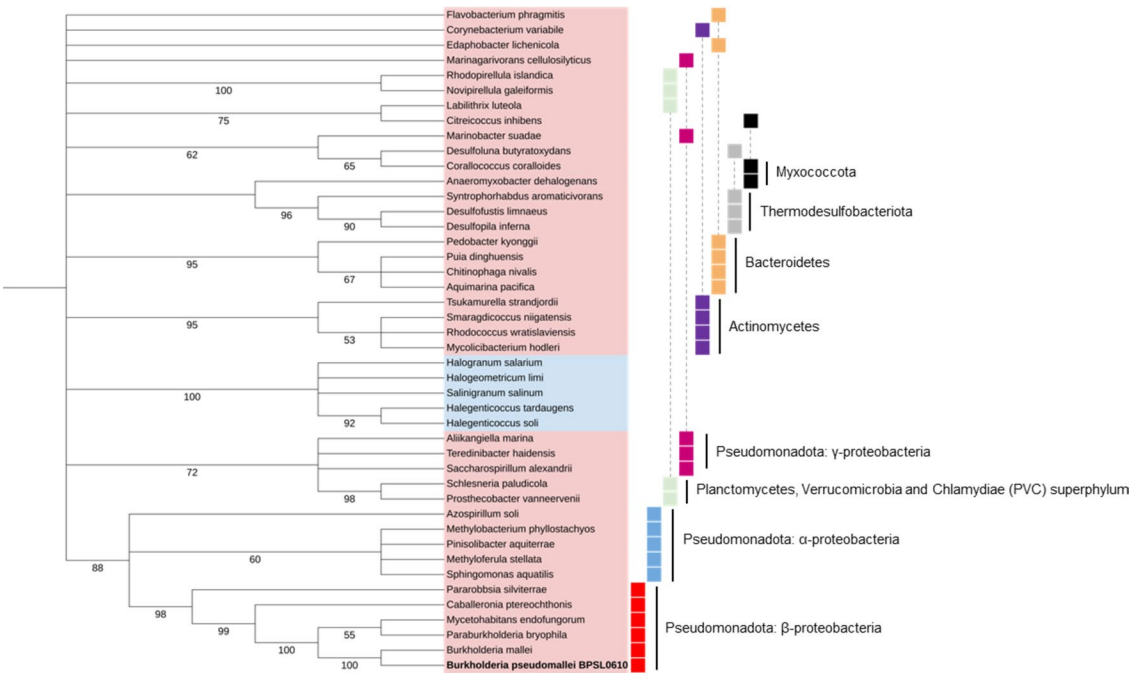


Fig. 2 Phylogenetic analysis of BPSL0610. A total of 45 species from 43 genera were represented in the tree based on the Blastp analysis of BPSL0610 against the RefSeq Select database. Nodes highlighted in red indicate species classified under the bacteria domain while nodes highlighted in blue indicate species classified under the archaea domain.

reflects the expected positional error of the residues, aligned with the pLDDT score, highlighting regions of lower confidence in the structure of BPSL0610 (Fig. 3D). Helices α_1 and α_4 at the N-terminus together with α_{16}-α_{18} at the C-terminus, correspond to regions with low PAE score. Notably, α_{14} that connects both domains together, was predicted with low confidence. The Ramachandran plot (Fig. 3E) showed that most residues in the BPSL0610 predicted model fall under the favoured region, indicating that the overall predicted model was of good quality.

Upon an initial overall inspection of the BPSL0610 model, it was clear that the N and C-terminal domains were predicted to adopt very similar structural folds that may be indicative of a sequence duplication within the linear amino acid sequence of the protein (Fig. 3F). However, both domains displayed distinct electrostatic surface potential in which residues 1-330 of the N terminal domain (BPSL0610^{N-ter}) have a predicted overall negative

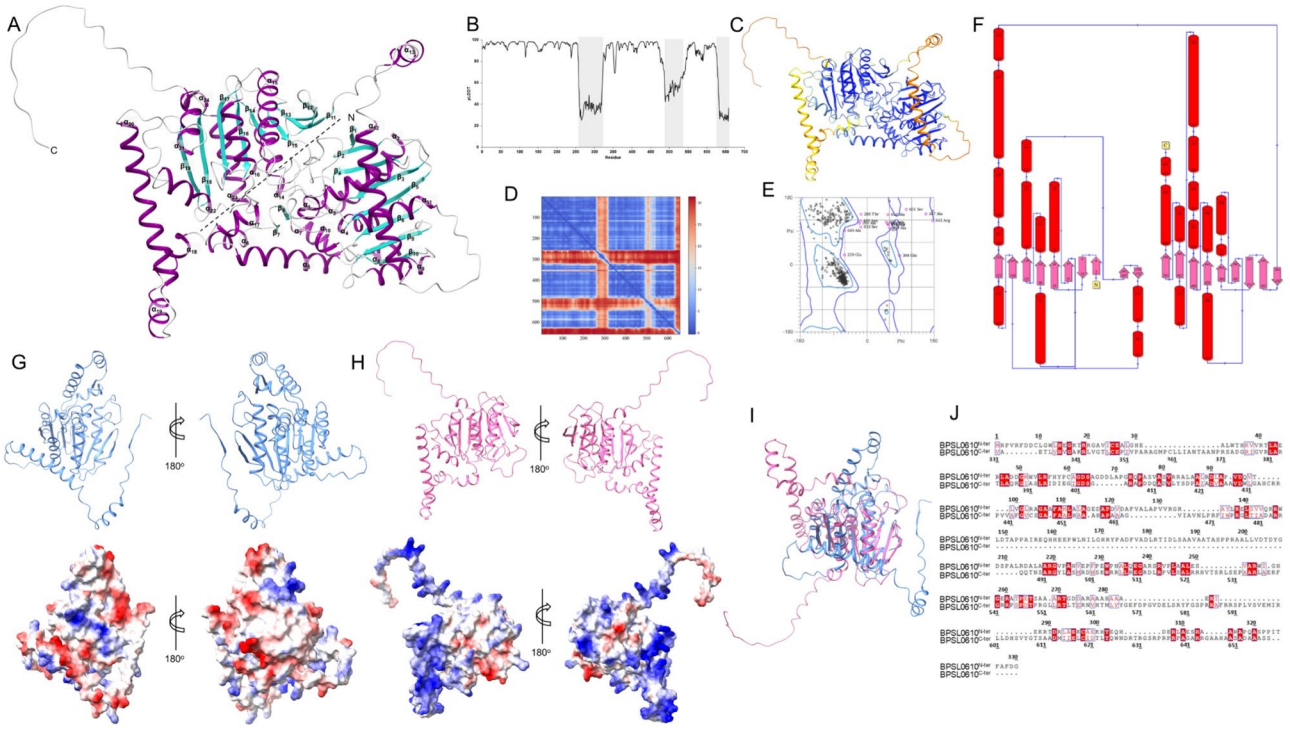


Fig. 3 The three-dimensional structure (3D) of BPSL0610 was predicted by AlphaFold2. **(A)** The 3D structure of BPSL0610 consists of 24 α helices (purple), 19 β-sheets (cyan) and loops (grey). The 3D structure of BPSL0610 shows a similar structural fold in the N-terminal and C-terminal regions. Dotted lines correspond to the point where the structure was split into two. The figure was generated with Chimera X [35]. **(B)**. Predicted local difference test (pLDDT), per-residue confidence score of BPSL0610. The shadowed regions represent a pLDDT score lower than 80, which indicates these regions are predicted at lower confidence. The overall model of BPSL0610 showed a pLDDT score greater than 80, indicating that these residues were predicted with high confidence. **(C)** The 3D structure of BPSL0610 is represented based on the pLDDT score in which blue regions correspond to a high pLDDT score while yellow and orange regions correspond to a low pLDDT score. **(D)** Predicted alignment error (PAE) score (high confidence blue; low confidence red). **(E)** Model quality assessment using MolProbity showed that 93.60% of the residues fall under the favoured region (blue) while 15 residues fall under the allowed region (purple). Outlines of the Ramachandran plot indicate the model is predicted at a good quality. **(F)** Topological diagram displaying the secondary structure of BPSL0610. Red cylinders represent α-helices while pink arrows denote β-sheets. The topology diagram of BPSL0610 displayed two α/β hydrolase fold domain at the N and C terminus. **(G)** 3D structure of the N-terminal half (BPSL0610^{N-ter}) consisting of residues 1 to 330. The surface electrostatic potential of BPSL0610^{N-ter} was represented by a blue surface, indicating a positive charge, while red corresponds to a negatively charged surface and white is neutral. **(H)** 3D structure and surface electrostatic potential of the C-terminal half (BPSL0610^{C-ter}), consisting of residues 331 to 658. **(I)** Superimposition of both halves, BPSL0610^{N-ter} (blue) and BPSL0610^{C-ter} (pink). **(J)** Pairwise alignment between the amino acid sequences of BPSL0610^{N-ter} and BPSL0610^{C-ter}. The sequences were aligned using T-COFFEE, and the alignment was visualised using ESPript 3.0. Fully conserved sequences are coloured red, while conserved sequences that are greater than the similarity global score (>0.7) are represented by a blue box.

charge, while residues 331–658 of the C terminal domain (BPSL0610^{C-ter}) were predicted to be more positively charged (Fig. 3G-H). The superimposition between BPSL0610^{N-ter} and BPSL0610^{C-ter} also showed that the central β-sheets of both structures were structurally aligned with an RMSD of 1.02 Å (55 Cα atoms of aligned residues) but outside of these regions, the structures were significantly different (Fig. 3I). Additionally, sequence alignment of the two domains together showed that they only shared 28% sequence identity (Fig. 3J) confirming that the predicted structure did not arise as a result of gene duplication.

Subsequent MD analysis showed that the Cα backbone of the BPSL0610 model displayed minimal deviation after 20 ns, with a RMSD of 0.4 Å over the 100 ns simulation showing that the model structure was structurally stable (**Supplementary Fig. 3A**). Nonetheless, high fluctuations in RMSF were observed in the regions of BPSL0610 that were predicted with low confidence by AlphaFold2 which include α_1, α_4, α_{16}, α_{17}, α_{18} and the loop located at the C-terminus (**Supplementary Fig. 3B-C**). In addition, the MD trajectory displayed a persistent inter-domain orientation between the two α/β hydrolase domains of BPSL0610 (**Supplementary Fig. 3C**). Such a configuration is unusual among the α/β hydrolase assemblies. Therefore, residues involved in the interaction between the N and C-terminal domains were determined based on a cut-off distance of 5 Å. The analysis revealed a predominance of hydrophobic residues within the inter-domain interface of 2483 Å^2, suggesting that the structural organisation of the two domains in BPSL0610 is mainly stabilised by hydrophobic interactions (**Supplementary Fig. 3D-E**). The stable inter-domain arrangement and interaction observed during the MD simulation also suggests that the relative organisation of the two domains is likely functionally relevant and may play a role in the formation and maintenance of theBPSL0610 active site.

Structural comparison of BPSL0610 with canonical α/β hydrolases

Canonical α/β hydrolases are constructed to present a catalytic triad at the heart of the protein fold. This usually consists of a nucleophile, histidine and an acidic residue, most commonly Ser-His-Asp[51]. To achieve this, the fold typically consists of a central β-sheet constructed from 5 to 11 β-strands, with the second β-strand often arranged in an antiparallel fashion[52]. This central β-sheet is then surrounded by α-helices, the number of which varies between proteins, to yield the overall fold[53]. The catalytic triad is then presented on intervening loops between secondary structure elements and usually represents the most conserved feature in the α/β hydrolase family[54]. There is considerable variation between enzymes in this large enzyme class, which often contain extended structural elements such as active site lids or caps which can be crucial for substrate specificity and enzymatic activity, or N or C-terminal accessory domains[53]. The predicted structure of BPSL0610, and the individual BPSL0610^{N-ter} and BPSL0610^{C-ter}, were compared against the protein structures in the PDB using the DALI server **(Supplementary Table 1)**. The search using the full-length structure revealed structural matches to single domain α/β hydrolase structures only, suggesting that the arrangement of the tandem α/β hydrolase domains in the full-length BPSL0610 could be novel. The comparison also revealed that structural matches to the BPSL0610^{N-ter} retained a higher Z-score compared to those that matched to the BPSL0610^{C-ter}, suggesting that the C-terminal domain may represent an α/β hydrolase domain that had not been previously structurally characterised **(Supplementary Table 1)**.

The features of the α/β hydrolase of BPSL0610^{N-ter} and BPSL0610^{C-ter} were compared with feruloyl esterase from *Candidatus bathyarchaeota* (PDB ID: 8B4U) as it displayed the highest structure similarity with BPSL0610 based on the DALI search (**Supplementary Table 1**). The *C. bathyarchaeota* feruloyl esterase contains the canonical α/β hydrolase and an extended lid domain[55]. The superposition between BPSL0610^{N-ter} and feruloyl esterase identified an addition of two α-helices and an extended lid domain (Arg_{132} – Ile_{183}) in BPSL0610^{N-ter}, composed of three α-helices and two antiparallel β-sheets (Fig. 4A). No extended lid or cap domain was found in BPSL0610^{C-ter} (Fig. 4B). Therefore, structural comparison of BPSL0610^{C-ter} with α/β hydrolases that lack the extended lid domain was conducted and showed that the eight central β-sheets in BPSL0610^{C-ter} were conserved and these central β-sheets are surrounded by seven α-helices (Fig. 4C). In addition, there was an insertion of four additional α-helices not observed in the canonical α/β hydrolase fold used for comparison (Fig. 4C). Most

of these extra α-helices insertion identified in both BPSL0610^{N-ter} and BPSL0610^{C-ter} corresponded to a low pLDDT score indicating that these regions were predicted at low confidence (Fig. 3C). With this in mind, we also analysed each of these domains for a likely catalytic triad that would be indicative of a potential activity for this unusual enzyme.

Identification of a putative active site and substrate binding pocket in BPSL0610

BPSL0610^{N-ter} and BPSL0610^{C-ter} were examined for potential active sites using the above structural comparisons and multiple sequence alignment (MSA) (Fig. 5A). Most reported esterase enzymes have a consensus G-X-S-X-G motif and a conserved Ser-His-Asp catalytic triad[56,57]. The MSA revealed that BPSL0610^{N-ter} appeared to have a disrupted motif consisting of ^{101}G-K-R-A-G^{105} in which the typical catalytical nucleophile, Ser was replaced by Arg (Fig. 5A). Structural analysis confirmed the position of this Arg and together with the MSA, also revealed that the key histidine typically involved in the catalytic triad was also missing in this domain. Indeed, superposition of the predicted BPSL0610^{N-ter} domain with a characterised esterase clearly showed that BPSL0610^{N-ter} cannot form a canonical active site and is thus unlikely to be active (Fig. 5B).

In BPSL0610^{C-ter}, the pentapeptide motif consists of ^{443}G-V-C-S-G^{447} and contains a cysteine residue (Cys_{445}) in place of the more typical catalytic serine that is found in many esterases. The other residues that would be expected to form a catalytic triad (His_{604} and Asp_{571}) also appeared to be conserved in the MSA (Fig. 5A). Replacement of the catalytic Ser with Cys is typically observed in thioesterases[58] and hence, the structure superimposition of BPSL0610^{C-ter} with the thioesterase GrgF from *Penicillium sp* was analysed. The residues were also structurally aligned with the nucleophile Cys_{445} that is predicted to be located in a sharp turn between the end of β_{13} and the beginning of α_{22} (Fig. 5C). The catalytic triad residues (Cys_{445}, His_{604} and Asp_{571}) are lined up in a row on one side of the putative active site cavity with hydrogen bonding distances suggesting that they should form a charge relay system as expected for a thioesterase[59].

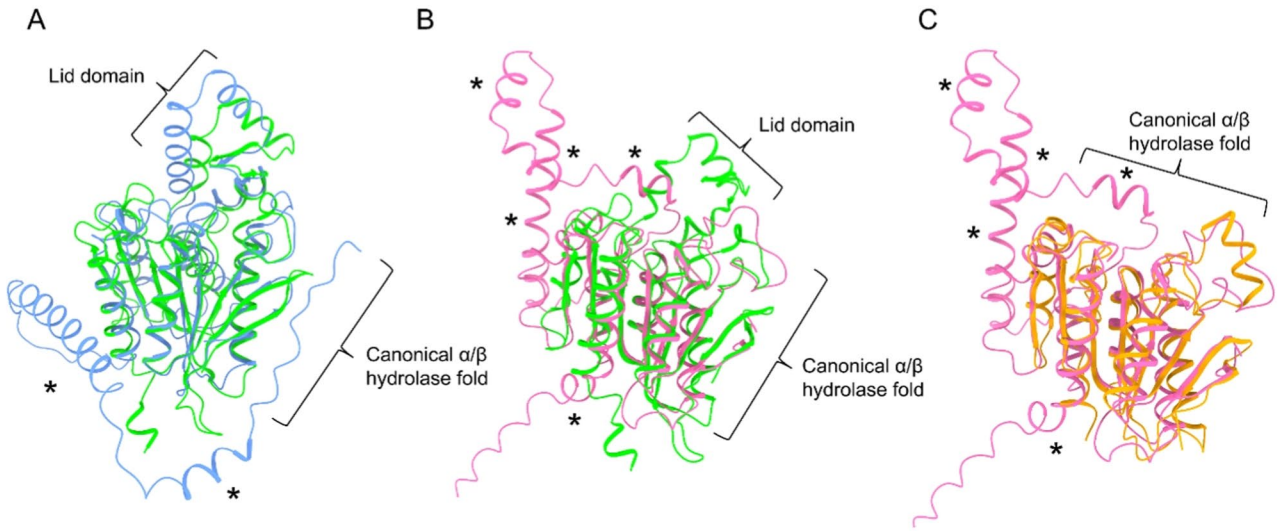


Fig. 4 Structure comparison of BPSL0610^{N-ter} and BPSL0610^{C-ter} with a canonical α/β hydrolase fold. Superimposition of the canonical α/β hydrolase fold of feruloyl esterase from *Candidatus bathyarchaeota* that contains an extended lid domain (PDB ID: 8B4U) (green) with **(A)** BPSL0610^{N-ter} (blue) and **(B)** BPSL0610^{C-ter} (pink). Structural comparison revealed that BPSL0610^{N-ter} shared high similarity to feruloyl esterase from *C. bathyarchaeota* with a RMSD of 0.9 Å (241 equivalent Cα atoms), compared to BPSL0610^{C-ter} with a RMSD of 1.2 Å (123 equivalent Cα atoms). **(C)** Superimposition of a canonical α/β hydrolase fold dienelactone hydrolase from *Anabaena variabilis*, lacking an extended lid domain (PDB ID: 2O2G) (orange) with BPSL0610^{C-ter} (pink), corresponded to a RMSD of 1.1 Å for 113 equivalent Cα atoms. The black * symbol denotes insertion of helices into the canonical α/β hydrolase fold domain.

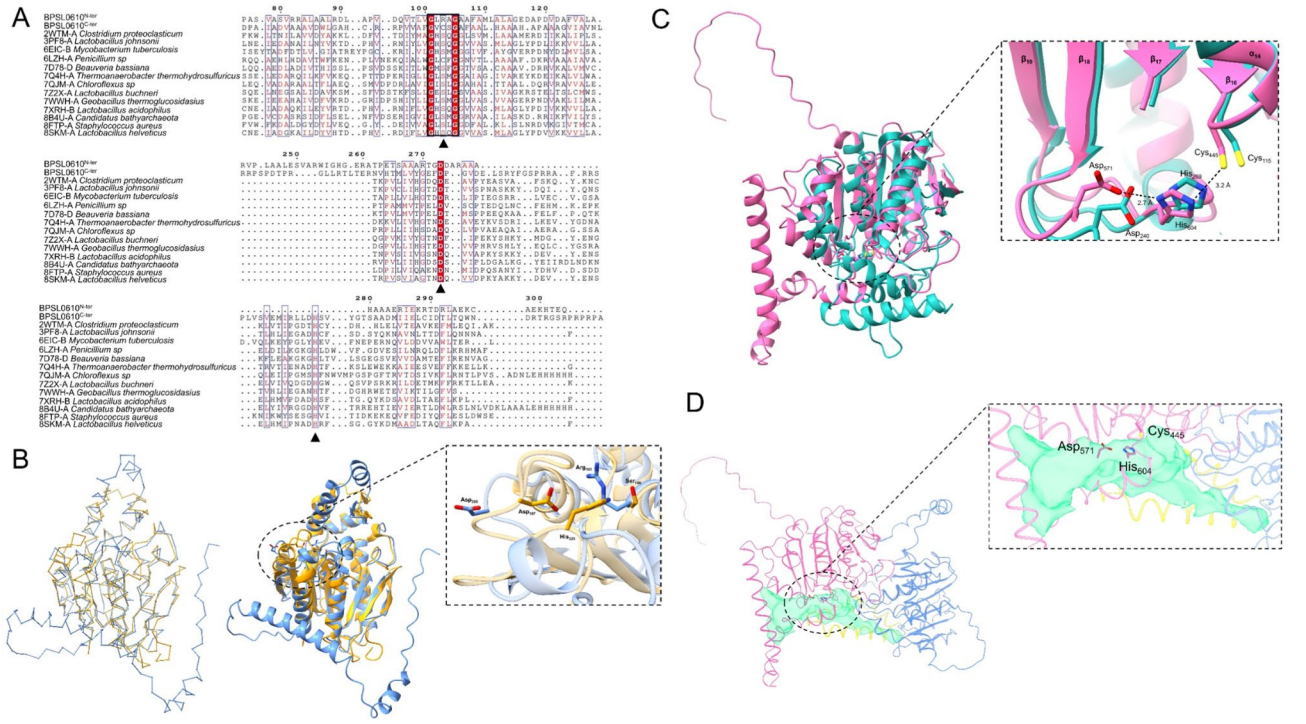


Fig. 5 Sequence and structure comparison of BPSL0610$^{N\text{-}ter}$ and BPSL0610$^{C\text{-}ter}$ with other structurally homologous proteins. **(A)** Multiple sequence alignment of BPSL0610$^{N\text{-}ter}$ and BPSL0610$^{C\text{-}ter}$ with α/β hydrolases identified using DALI. The sequences were aligned using T-COFFEE, and the alignment was visualised using ESPript 3.0. Fully conserved sequences are coloured red, conserved sequences that are greater than the similarity global score (>0.7) are represented by a blue box, while the black box indicates the conserved motif sequence, GXSXG (where X represents any residue). Arrowheads represent residues that typically form the catalytic triad in esterase with this fold. **(B)** The superimposition between BPSL0610$^{N\text{-}ter}$ (blue) and esterase (orange) from *Lactobacillus johnsonii* PDB ID: 3PF8, corresponds to a RMSD of 0.9 Å for 107 equivalent Cα atoms. The close-up view of the catalytical triad Ser_{106}, His_{225} and Asp_{197} of esterase is equivalent to Arg_{103} and Asp_{205} of BPSL0610, respectively. **(C)** Superposition between BPSL0610$^{C\text{-}ter}$ (pink) and thioesterase GrgF from *Penicillium sp.* PDB ID: 6LZH (cyan). The superposed structure corresponds to a RMSD of 1.0 Å for 102 equivalent Cα atoms. Insert is a close-up view of the superimposition in the active site. Cys_{115}, His_{269} and Asp_{240} represents the catalytic triad in the thioesterase and are shown as sticks. The equivalent residues (Cys_{445}, His_{604} and Asp_{571}) are also shown for BPSL0610. **(D)** The identified cavity (green, volume of 1943 $Å^3$) formed around the proposed active site (residues show as sticks). BPSL0610$^{C\text{-}ter}$ is shown in pink and BPSL0610$^{N\text{-}ter}$ is coloured blue with the lid domain shown in yellow.

In addition, examination of the full-length protein structure revealed a shared putative substrate binding pocket between BPSL0610^{N-ter} and BPSL0610^{C-ter} domains with the lid domain of BPSL0610^{N-ter} positioned between the two α/β hydrolase domains. The cavity that forms the substrate binding pocket exhibited a volume of 1942 $Å^3$, which is enriched with hydrophobic residues, with polar residues distributed within the cavity (Fig. 5D). The identified shared putative substrate binding pocket suggests that both α/β hydrolase domains could be required to accommodate potential substrates that access the active site of BPSL0610.

Structure prediction of BPSL0610-ACP-4′-phosphopantetheine (4′-PP) ternary complex

The thioesterase domain has been reported to catalyse the hydrolysis of thioester bonds between the substrate and the 4'-PP to release the substrate from the carrier protein (ACP)[60]. Our analysis suggests that BPSL0610 is a thioesterase and given the co-localisation of *bpsl0610* with the gene encoding for ACP contained within the *becA-R* gene locus, we investigated whether these proteins interact. Protenix-v1 [41] and RoseTTAFold3 [42] were used to predict whether a ternary complex could be formed between BPSL0610 and the ACP (BPSL0615). As

part of this modelling, the ACP was phosphopantethenylated on Ser_{52}, which is critical for its function. We noted that, the residue Ser_{52} of the AlphaFold2 predicted BPSL0615 was structurally conserved with Ser_{42} of *Bradyrhizobium japonicum* ACP protein (PDD ID: 4H2U) (**Supplementary Fig. 4**). Both ternary complexes obtained from Protenix-v1 and RoseTTAFold3 were predicted at high confidence. The ternary complex model predicted using Protenix-v1 recorded a pLDDT score of 81.5, pTM and iPTM scores of 0.98 (**Supplementary Fig. 5A**). The predicted ternary complex model from RoseTTAFold3 corresponded to a pLDDT score of 82, a pTM score of 0.79, and an iPTM score of 0.81, likewise indicating high confidence of the predicted structure and protein–substrate interface (**Supplementary Fig. 5B**). Furthermore, a low PAE score observed at the active site region of both complexes further supports that the positions of most of the residues within the active site of BPSL0610 and the phosphopantetheine (4'-PP) were predicted with high confidence. The superposition of both complexes revealed a similar protein-protein interaction (PPI) and binding orientation, in which the 4'-PP was positioned towards the active site of BPSL0610 (**Supplementary Fig. 6**). Overall, the comparable binding orientation which is observed in the predicted model from both servers supports the consistency of the predicted binding pose. Nevertheless, three regions adopted a distinct conformation in the models generated by both servers. Notably the α_{19} helix region that is positioned close to the ACP showed a considerable positional variation between the predicted structures, suggesting that this region is conformationally dynamic. The remaining distinct conformation observed at the peripheral region of $BPSL0610^{N-ter}$ and $BPSL0610^{C-ter}$ domains respectively. However, owing to their peripheral locations, these variations observed are unlikely to disrupt the structural integrity between BPSL0610 and ACP. Given that the complex ternary structure predicted using Protenix-v1 server had a high pTM and iPTM scores, the model was selected for additional analysis.

The predicted complex structure of BPSL0610-ACP was then compared against the protein structure of a thioesterase-peptidyl carrier protein complex (PCP-TE) from *Paraburkholderia acidicola* (PDB ID: 8W2D) which functions in the biosynthesis of the NRPS derived natural product sulfazecin[61]. Superposition of both complex structures showed that the canonical α/β hydrolase fold and the catalytic triad of both thioesterase domains in BPSL0610-BPSL0615-4'-PP and PCP-TE complex is conserved (Fig. 6A). However, the ACP domain of the ternary complex was not conserved with the PCP domain. Instead, both carrier proteins displayed different orientations when interacting with the thioesterase domain of both complexes (Fig. 6B-C). Nonetheless, the 4'-PP in the BPSL0610-BPSL0615-4'-PP complex and the PCP-TE complex structure presented a similar orientation to enter the active site of the thioesterase domain (Fig. 6D). The sulfhydryl group of 4'-PP approached the catalytic site residue Cys_{445} of BPSL0610 in close proximity (2.7 Å apart) (Fig. 6D). Furthermore, the 4'-PP was able to access the catalytic Cys_{445} through a phosphopantetheine tunnel which predominantly consists of hydrophobic residues (from $BPSL0610^{N-ter}$ and $BPSL0610^{C-ter}$ domains) that may guide the 4'-PP towards the active site, similar to PCP-TE [58] (Fig. 6E). The ACP domain was shown to interact with the lid domain of BPSL0610 encompassing approximately 1272 $Å^2$ of total buried surface area (Fig. 6F). A similar size interaction interface was observed in the PCP-TE complex of *Escherichia coli* K-12 [62]. Furthermore, the ACP domain also interacts with the $BPSL0610^{N-ter}$ and $BPSL0610^{C-ter}$ domains through the (i) interface between both α/β hydrolase domains predominantly mediated by electrostatic interaction, and (ii) the lid domain of $BPSL0610^{N-ter}$ via hydrophobic interaction (Fig. 6F).

In addition, the stability of the predicted ternary complex was further evaluated through MD simulations and the results showed that the complex had only undergone minimal structural deviation after 20 ns with an average RMSD of ~2.8 Å (**Supplementary Fig. 7A**). Notably, the 4'-PP prosthetic group remained positioned within the active site of BPSL0610 and maintained a distance ranging from ~1.5 to 8 Å (average of 5.6 Å) between the sulphur (Sγ) atom of the proposed catalytic cysteine (Cys_{445}) over a 100 ns simulation (**Supplementary Fig. 7B**). Furthermore, the ACP domain maintained a constant interaction with the lid domain of BPSL0610 throughout the simulation (**Supplementary Fig. 7C**). The ACP protein remained structurally stable and exhibited no substantial conformational changes throughout the MD simulation. Nonetheless, ACP binding was associated with conformational changes in the structure of BPSL0610, suggesting structural adaptation of BPSL0610 to accommodate the interaction with ACP (**Supplementary Fig. 7D-E**). Superimposition of the apo and ternary

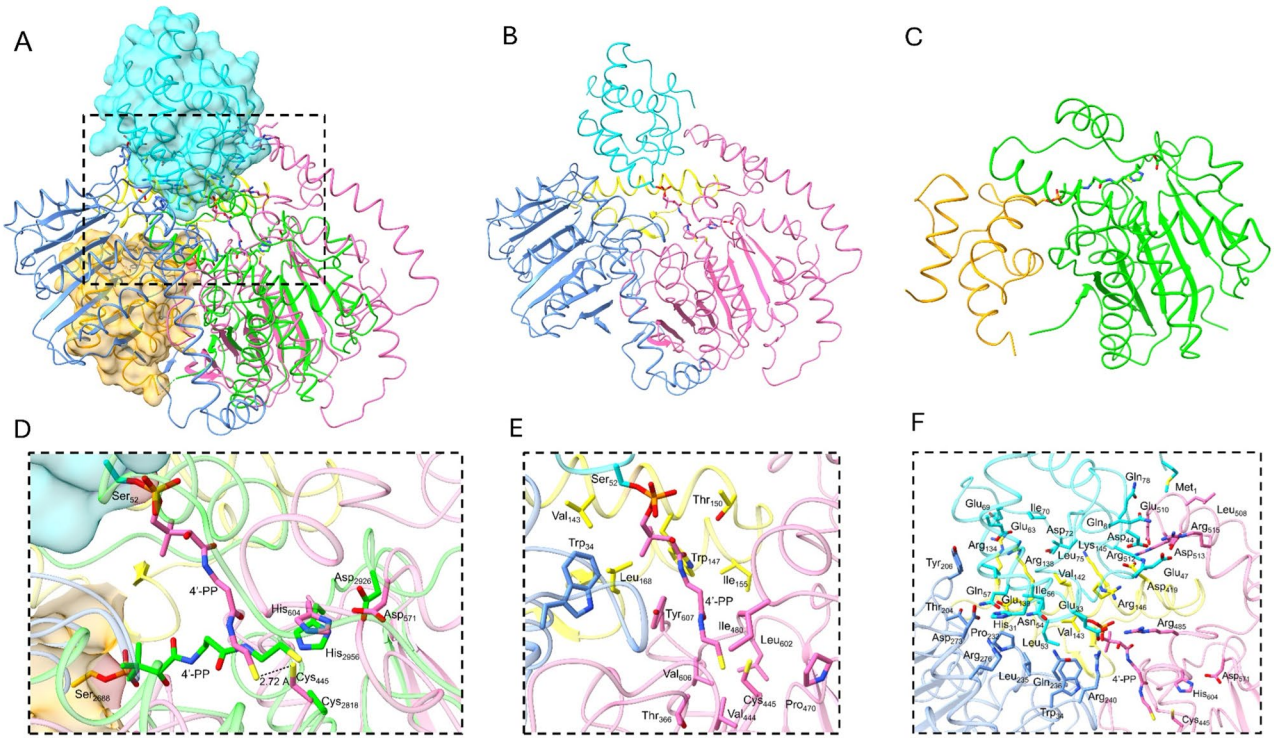


Fig. 6 Structural analysis of the predicted BPSL0610-BPSL0615 complex. **(A)** BPSL0610 is shown with BPSL0610$^{N\text{-ter}}$ coloured blue and BPSL0610$^{C\text{-ter}}$ coloured pink. The lid domain present in BPSL0610$^{N\text{-ter}}$ is coloured yellow. BPSL0615 is shown in cyan with its molecular surface shown. This structure was superimposed with the thioesterase (green) from the PCP-TE complex from *Paraburkholderia acidicola* (PDB ID: 8W2D). The PCP from this complex is shown in orange with the molecular surface displayed once again. The superimposition of both complexes corresponds to RSMD of 1.3 Å for 37 equivalent Cα atoms. **(B)** Protenix-V1 predicted structure of BPSL0610-BPSL0615 complex and **(C)** PCP-TE complex (PDB ID: 8W2D) were presented with orientation and domain colour schemes as shown in (A). **(D)** The close-up view of the active site in the superposition. The catalytic triad Cys_{2818}, His_{2956} and Asp_{2926} of the thioesterase domain from PCP-TE complex is equivalent to Cys_{445}, His_{604} and Asp_{571} of BPSL0610, respectively. In both BPSL0610-BPSL0615 complex and PCP-TE complex the 4'-PP extends into the catalytic pocket and is oriented towards the catalytic cysteine. **(E)** The predicted phosphopantetheine tunnel which composed mostly hydrophobic residues allowing the 4'-PP to enter the active site of BPSL0610. **(F)** The interdomain contact residues (within a 3.5 Å distance cut off) predicted between the ACP domain (cyan) and the lid domain (yellow).

structures after 100 ns of MD simulation identified three conformationally variable regions that coincided with high-RMSF segments (**Supplementary Fig. 7E**). These identified flexible segments are consistent to the distinct conformations observed between the ternary complex model predicted by Protenix-v1 and RoseTTAFold3 (**Supplementary Fig. 6**). Notably, the α_{19} helix region is shifted towards the ACP. The lower RMSF observed at α_{19} helix of the ternary structure compared to the apo structure suggests that it adopted a more stable conformation during the ternary complex formation. The remaining flexible regions are located peripherally to BPSL0610^{N-ter} and BPSL0610^{C-ter} domains. (**Supplementary Fig. 7E**). Overall, the MD simulation revealed a conformational change in BPSL0610 upon ternary complex formation.

Expression and purification of rBPSL0610^{MBP}

To begin the experimental characterisation of BPSL0610, the protein was recombinantly produced as rBPSL0610^{MBP}. The recombinant protein was purified using a three-step purification approach consisting of affinity chromatography followed by size exclusion chromatography and MBP Trap chromatography (**Supplementary Fig. 8A-C**). The purity of rBPSL0610^{MBP} was validated through SDS-PAGE which displayed the

presence of minor contaminants which may represent host proteins or signs of protein degradation (**Supplementary Fig. 8C**). The solution containing proteins from the peak fractions were therefore digested with trypsin before being subjected to verification using LC-MS/MS. A total of 24 peptides were identified in which 21 peptides correspond to 30% of the sequence coverage of BPSL0610 and three peptides accounting for MBP were identified, confirming that the target recombinant enzyme had been successfully produced (**Supplementary Fig. 9 and Supplementary Table 2**). As indicated above, the additional protein bands identified below the target protein size of rBPSL0610^{MBP} (~116 kDa) in the SDS-PAGE (**Supplementary Fig. 8C**), are likely associated with rBPSL0610^{MBP} protein degradation as supported by the MS readout.

Determination of esterase activity for rBPSL0610^{MBP}

Since the structure prediction analysis has suggested BPSL0610 was likely a (thio)esterases, general *p*-NP esters of aliphatic side chains lengths (*p*NP-C2, *p*NP-C4, *p*NP-C6 and *p*NP-C10) were evaluated as substrates for the enzyme using an esterase assay. The release of *p*-nitrophenol from these substrates was monitored against time by measuring the absorbance at OD_{410}. (Fig. 7). The rBPSL0610^{MBP} showed detectable catalytic activity despite showing low activity compared to lipase used as a control (Fig. 7A and **Supplementary Fig. 10**). rBPSL0610^{MBP} displayed catalytic activity towards *p*NP-C2 to *p*NPC6 with the highest activity noted towards the shortest substrate, *p*NP-C2. Enzyme activity declined steadily as the number of carbon atoms in the acyl chain increased until no detectable activity could be seen with *p*NP-C10 (Fig. 7B). Hence, these results confirm that rBPSL0610^{MBP} is capable to have esterase activity.

The kinetics parameters of rBPSL0610 were calculated to determine the K_m, V_{max} and k_{cat} values for the reaction catalysed by rBPSL0610^{MBP}. (Fig. 7). The analysis showed that the K_M value decreases as the aliphatic side chain length of the substrate increases. Furthermore, the enzyme was shown to have a high turnover rate (k_{cat}) towards short chain substrates (*p*NP-C2-C4) (Table 1). Nonetheless, rBPSL0610^{MBP} exhibits high preferential and catalytic efficiency towards *p*NP-C4, presenting the highest k_{cat}/K_M value of 2.1×10^4 mM^{-1} s^{-1} and V_{max}/K_M value of 1.83 µmol min^{-1} mM^{-1}. In contrast, *p*NP-C6 displayed the lowest k_{cat}/K_M value of 2.0×10^2 mM^{-1} s^{-1} and V_{max}/K_M value of 1.05 µmol min^{-1} mM^{-1} despite having the lowest K_M. This kinetics pattern of

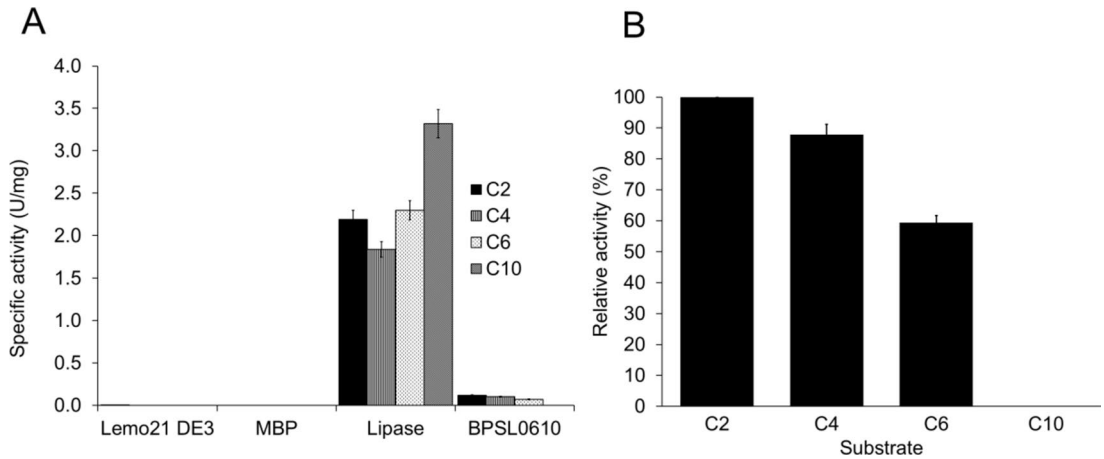


Fig. 7 Substrate specificity of rBPSL0610^{MBP} using *p*NP substrates. **(A)** Control reactions for the *p*NP substrate specificity assay. Control assay consisting of *E. coli* Lemo21 DE3 lysate and MBP protein as negative control while porcine pancreatic lipase was used as a positive control. Assay was conducted at 37 °C using *p*NP-C2, *p*NP-C4, *p*NP-C6 and *p*NP-C10 at a uniform concentration of 10 mM. The specific activity (U/mg) was shown as mean ± SE of three independent assays. Catalytic activity was absent for lysate and the MBP protein. **(B)** The maximal enzymatic activity of rBPSL0610^{MBP} was defined as 100% and the relative activity was shown as the percentage of maximal enzymatic activity (mean ± SE of three independent assays).

Table 1 Enzyme kinetics parameters for rBPSL0610^{MBP}.

Substrates	K_m (mM)	V_{max} (μmol min^{-1})	k_{cat} (s^{-1})	k_{cat}/K_M (mM^{-1} s^{-1})	V_{max}/K_m (μmol min^{-1} mM^{-1})
*p*NP-C2	8.6 ± 0.5	11.8 ± 0.2	1.37×10^5	1.6×10^4	1.38
*p*NP-C4	4.1 ± 0.9	7.1 ± 0.3	8.19×10^4	2.1×10^4	1.83
*p*NP-C6	2.6 ± 0.1	2.8 ± 0.01	5.32×10^2	2.0×10^2	1.05

rBPSL0610^{MBP} that displays highest affinity towards medium aliphatic acyl length of *p*NP ester, but exhibits the lowest hydrolysis, was observed similar to EstM2 esterase derived from a metagenome soil bacteria and EstC esterase from *Streptomyces coelicolor* A3(2)[63,64].

Discussion

BPSL0610 was predicted to function as a thioesterase (TE) based on sequence and structure homology with proteins classified under the α/β hydrolase superfamily. The α/β hydrolase family is one of the largest groups comprising of structurally related enzymes with diverse functions[65]. The predicted 3D structure of BPSL0610 displayed characteristics similar to TEs (EC 3.1.2) which mediate the hydrolysis of a thioester bond between a carbonyl group and a sulphur atom[66]. TEs are vital in many biosynthetic pathways as they typically catalyse the final step to release a biosynthetic product from an activated acyl-coenzyme A (CoA) or acyl-carrier protein (ACP). They typically function in fatty acid biosynthesis, polyketide and non-ribosomal peptide production[67], but here, BPSL0610 is predicted to have a role in an experimentally unverified exopolysaccharide modification machinery.

The present analysis showed that BPSL0610 is predicted to form two similar α/β hydrolase domains at the N and C terminal (Fig. 3). Comparison of each domain with the canonical α/β hydrolase fold identified a conserved lid domain in BPSL0610^{N-ter} which was not present in BPSL0610^{C-ter} (Fig. 4D). The identified lid domain is predicted to help form a potential binding pocket bridging the BPSL0610^{N-ter} and BPSL0610^{C-ter} domains. The lid domain may therefore be crucial in coordinating substrates towards the active site of the thioesterase[62]. Formation of the potential binding pocket between two α/β hydrolase domains has never been reported before to our knowledge, which suggests that this predicted model may represent a novel structural arrangement within the α/β hydrolase superfamily. α/β hydrolase-mediated hydrolysis is generally achieved using a catalytic triad composed of a nucleophile (serine, cysteine, or aspartate), a strictly conserved histidine and an acidic residue[68–70]. In addition, these catalytic residues are always arranged in the order of nucleophile, acidic residue, and histidine in the primary sequence[69]. The catalytic nucleophile is usually located between the fifth β-sheet and α-helices in a strained gamma turn conformation, frequently known as the nucleophile elbow[69,70]. Such a triad was not found in the N-terminal domain of the protein but was present in the C-terminal domain (Cys_{445}, His_{604} and Asp_{571}) suggesting that this is the likely site of catalysis. Indeed, the predicted structure shows that the nucleophilic Cys_{445} is located between the end of strand β_4 and the beginning of α_{22}, forming the nucleophile elbow (Fig. 5).

The αβ hydrolase fold of TEs is typically involved in the termination of chain elongation in an ACP-dependent biosynthetic process by hydrolysing the thioester linkages between a substrate and the 4'-PP arm of the ACP[71,72]. In such systems, the active site of the TE recognises a specific substrate that bound to the ACP domain and cleaves the substrate-4'PP-ACP thioester bond once the chain elongation process is complete[73]. Given that BPSL0610 is likely a α/β hydrolase fold type thioesterase and shares structural similarity to the GrgF thioesterase (Fig. 5C) that is involved in the synthesis of the polyketide[74], it is possible that BPSL0610 may facilitate the hydrolysis of substrates tethered to BPSL0615 (ACP) during exopolysaccharide modification. This hypothesis was further supported by a prediction of a complex between BPSL0610 and ACP (BPSL0615) that was predicted at high confidence (**Supplementary Fig. 5**).

Interactions between thioesterases and ACP/PCPs in NRPS systems have been reported in several experimentally determined structures[61,62,75,76]. In these structures, the PCP domain adopts various orientations during its

interaction with the TE domain. The interaction between the PCP domains with the lid domain of TE stabilised the conformation of the lid domain, which in turn facilitated the organisation of the substrate channel and catalytic environment of the TE domain. This then enabled the accommodation of the substrate bound to the 4'-PP within the active site of thioesterase[62]. Interestingly, in this study, the 4'-PP attached to the ACP was predicted to enter the proposed active site of BPSL0610 with the terminal sulfhydryl group in close proximity to the catalytic cysteine. Indeed, the sulfhydryl is positioned at a similar distance to the cysteine as compared to a PCP-TE complex from *P. acidicola*, despite a major difference in the orientation of the ACP domain (Fig. 6A).

The interaction between the ACP and BPSL0610 also appeared to be mediated by the lid domain present in BPSL0610^{N-ter}, presenting additional insight into the mode of action of this enzyme. Taken together, the predicted high confidence BPSL0610-BPSL0615 ternary complex structure and the MD simulation analysis suggest that BPSL0610 may function as a thioesterase to facilitate the release of an amino-acyl amino moiety from the ACP through hydrolysis of the thioester bond.

Conclusion

In conclusion, the 3D structure of BPSL0610 was predicted with high confidence using an ab initio structure prediction approach. The predicted structure revealed the presence of two similar α/β hydrolase domains located at the BPSL0610^{N-ter} and BPSL0610^{C-ter}. Structure comparison indicates that both domains share significant similarities with a variety of esterases. However, only the BPSL0610^{C-ter} domain retains a conserved catalytic triad. The esterase assay further supported the role of the nucleophilic Cys_{445} in hydrolysing short-chain substrates. Furthermore, the BPSL0610^{N-ter} contains a conserved lid domain. The predicted structure of a ternary complex between BPSL0610 and BPSL0615 further suggested that the lid domain may be crucial for the binding of the ACP. The esterase activity detected in rBPSL0610^{MBP} also strengthened the proposed functional role of the putative conserved catalytic triad in catalysing the hydrolysis of ester bonds. Taken together, these data suggest that BPSL0610 most likely functions as a thioesterase and given the genomic location of its gene, may act in concert with the enzymes encoded in the AAL-cassette as part of the exopolysaccharide biosynthetic machinery in BP.

Supplementary Information The online version contains supplementary material available at https://doi.org/10.1038/s41598-026-72746-x.

Acknowledgements We thank Dr Maizom Hassan, Dr Izyanti Ibrahim and Dr Ahmad Faris Seman Kamarulzaman for their useful discussion.

Author contributions Pravin Kumran Nyanasegran: Conceptualization, Data curation, Analysis, Investigation, Methodology, Resources, Visualization, Validation, Writing – original draft and editing. Jia Rong Tey: Investigation, Methodology - reviewing & editing. Anis Nadyra Zifruddin: Analysis, Investigation, Methodology - reviewing & editing. JiaXian Ong: Investigation, Methodology. Sheila Nathan: Supervision, Project administration, Writing – review & editing. Glyn R Hemsworth: Conceptualization, Investigation, Writing – review & editing. Mohd Firdaus Raih: Supervision, Funding acquisition, Writing – review & editing. Nor Azlan Nor Muhammad: Supervision, Resources, Writing – review & editing. Chyan Leong Ng: Conceptualization, Data curation, Funding acquisition, Analysis, Investigation, Methodology, Resources, Visualization, Writing - reviewing and editing.

Funding This work is supported by Geran Universiti Penyelidikan (GUP), Universiti Kebangsaan Malaysia, Malaysia [Grant number: GUP-2021-069].

Data availability Data is provided within the manuscript or supplementary information files.

Declarations

Competing interests The authors declare no competing interests.

Open Access This article is licensed under a Creative Commons Attribution 4.0 International License, which permits use, sharing, adaptation, distribution and reproduction in any medium or format, as long as you give appropriate credit to the original author(s) and the source, provide a link to the Creative Commons licence, and indicate if changes were made. The images or other third party material in this article are included in the article's Creative Commons licence, unless indicated otherwise in a credit line to the material. If material is not included in the article's Creative Commons licence and your intended use is not permitted by statutory regulation or exceeds the permitted use, you will need to obtain permission directly from the copyright holder. To view a copy of this licence, visit http://creativecommons.org/licenses/by/4.0/.

References

1. Mariappan, V. et al. Hijacking of the host's immune surveillance radars by *Burkholderia pseudomallei*. *Front. Immunol.* **12**, 1–13 (2021).
2. Wiersinga, W. J. et al. Melioidosis. *Nat. Rev. Dis. Primers* **4**, 7108 (2018).
3. Yip, C. H., Ghazali, A. K. & Nathan, S. Burkholderia pseudomallei pathogenesis and survival in different niches. *Biochem. Soc. Trans.* **48**, 569–579 (2020).
4. Limmathurotsakul, D. et al. Role of Burkholderia pseudomallei biofilm formation and lipopolysaccharide in relapse of melioidosis. *Clin. Microbiol. Infect.* **20**, O854–O856 (2014).
5. Neopane, P., Nepal, H. P., Shrestha, R., Uehara, O. & Abiko, Y. In vitro biofilm formation by Staphylococcus aureus isolated from wounds of hospital-admitted patients and their association with antimicrobial resistance. *Int. J. Gen. Med.* **11**, 25–32 (2018).
6. Yan, J. & Bassler, B. L. Surviving as a community: antibiotic tolerance and persistence in bacterial biofilms. *Cell. Host Microbe*. **26**, 15–21 (2019).
7. Flemming, H. C. EPS Then and now. *Microorganisms* **4**, 41 (2016).
8. Peng, N. et al. The exopolysaccharide–eDNA interaction modulates 3D architecture of Bacillus subtilis biofilm. *BMC Microbiol.* **20**, 115 (2020).
9. Vestby, L. K., Grønseth, T., Simm, R. & Nesse, L. L. Bacterial biofilm and its role in the pathogenesis of disease. *Antibiotics* **9**, 59 (2020).
10. Chin, C. Y. et al. Global transcriptional analysis of Burkholderia pseudomallei high and low biofilm producers reveals insights into biofilm production and virulence. *BMC Genom.* **16**, 1–15 (2015).
11. Borlee, G. I. et al. Genome-scale analysis of the genes that contribute to Burkholderia pseudomallei biofilm formation identifies a crucial exopolysaccharide biosynthesis gene cluster. *PLoS Negl. Trop. Dis.* **11**, 1–29 (2017).
12. Mangalea, M. R., Plumley, B. A. & Borlee, B. R. Nitrate sensing and metabolism inhibit biofilm formation in the opportunistic pathogen Burkholderia pseudomallei by reducing the intracellular concentration of c-di-GMP. *Front. Microbiol.* **8**, 353 (2017).
13. Pakkulnan, R. et al. Extracellular DNA facilitates bacterial adhesion during Burkholderia pseudomallei biofilm formation. *PLoS One*. **14**, 1–19 (2019).
14. Winsor, G. L. et al. The Burkholderia Genome Database: facilitating flexible queries and comparative analyses. *Bioinformatics* **24**, 2803–2804 (2008).
15. Simunović, V. Genomic and molecular evidence reveals novel pathways associated with cell surface polysaccharides in bacteria. *FEMS Microbiol. Ecol.* **97**, fiab119 (2021).
16. Simunović, V. & Grubišić, I. Amino acid (acyl carrier protein) ligase-associated biosynthetic gene clusters reveal unexplored biosynthetic potential. *Mol. Genet. Genomics*. **298**, 49–65 (2023).
17. Holmquist, M. Alpha beta-hydrolase fold enzymes structures, functions and mechanisms. *Curr. Protein Pept. Sci.* **1**, 209–235 (2000).
18. Mei, G. Y., Yan, X. X., Turak, A., Luo, Z. Q. & Zhang, L. Q. AidH, an alpha/beta-hydrolase fold family member from an Ochrobactrum sp. strain, is a novel N-acylhomoserine lactonase. *Appl. Environ. Microbiol.* **76**, 4933–4942 (2010).
19. Mukherjee, S., Moustafa, D., Smith, C. D., Goldberg, J. B. & Bassler, B. L. The RhlR quorum-sensing receptor controls Pseudomonas aeruginosa pathogenesis and biofilm development independently of its canonical homoserine lactone autoinducer. *PLoS Pathog*. **13**, e1006504 (2017).
20. Little, D. J. et al. The protein BpsB is a poly-β-1,6-N-acetyl-D-glucosamine deacetylase required for biofilm formation in Bordetella bronchiseptica. *J. Biol. Chem.* **290**, 22827–22840 (2015).
21. Little, D. J. et al. The structure- and metal-dependent activity of Escherichia coli PgaB provides insight into the partial de-N-acetylation of poly-β-1,6-N-acetyl- D-glucosamine. *J. Biol. Chem.* **287**, 31126–31137 (2012).
22. Little, D. J. et al. PgaB orthologues contain a glycoside hydrolase domain that cleaves deacetylated poly-β (1, 6)-N-acetylglucosamine and can disrupt bacterial biofilms. *PLoS Pathog*. **14**, e1006998 (2018).

23. Wilhelm, S., Gdynia, A., Tielen, P., Rosenau, F. & Jaeger, K. E. The autotransporter esterase EstA of Pseudomonas aeruginosa is required for rhamnolipid production, cell motility, and biofilm formation. *J. Bacteriol.* **189**, 6695–6703 (2007).
24. Pan, S., Erdmann, M., Terrell, J. & Cabeen, M. T. A putative lipase affects Pseudomonas aeruginosa biofilm matrix production. *mSphere* **8**, e00374–e00323 (2023).
25. Bi, H., Christensen, Q. H., Feng, Y., Wang, H. & Cronan, J. E. The Burkholderia cenocepacia BDSF quorum sensing fatty acid is synthesized by a bifunctional crotonase homologue having both dehydratase and thioesterase activities. *Mol. Microbiol.* **83**, 840–855 (2012).
26. Altschul, S. F., Gish, W., Miller, W., Myers, E. W. & Lipman, D. J. Basic local alignment search tool. *J. Mol. Biol.* **215**, 403–410 (1990).
27. Thompson, J. D., Higgins, D. G. & Gibson, T. J. CLUSTAL W: improving the sensitivity of progressive multiple sequence alignment through sequence weighting, position-specific gap penalties and weight matrix choice. *Nucleic Acids Res.* **22**, 4673–4680 (1994).
28. Tamura, K., Stecher, G. & Kumar, S. MEGA11: Molecular Evolutionary Genetics Analysis Version 11. *Mol. Biol. Evol.* **38**, 3022–3027 (2021).
29. Le, S. Q. & Gascuel, O. An improved general amino acid replacement matrix. *Mol. Biol. Evol.* **25**, 1307–1320 (2008).
30. Letunic, I. & Bork, P. Interactive Tree Of Life (iTOL) v5: an online tool for phylogenetic tree display and annotation. *Nucleic Acids Res.* **49**, W293–W296 (2021).
31. Blum, M. et al. InterPro: the protein sequence classification resource in 2025. *Nucleic Acids Res.* **53**, D444–D456 (2025).
32. Jumper, J. et al. Highly accurate protein structure prediction with AlphaFold. *Nature* **596**, 583–589 (2021).
33. Mirdita, M. et al. ColabFold: making protein folding accessible to all. *Nat. Methods*. **19**, 679–682 (2022).
34. Williams, C. J. et al. MolProbity: More and better reference data for improved all-atom structure validation. *Protein Sci.* **27**, 293–315 (2018).
35. Pettersen, E. F. et al. UCSF Chimera-a visualization system for exploratory research and analysis. *J. Comput. Chem.* **25**, 1605–1612 (2004).
36. Laskowski, R. A. et al. Structural summaries of PDB entries. *Protein Sci.* **27**, 129–134 (2018).
37. Holm, L. Using Dali for protein structure comparison. *Struct. Bioinformatics: Methods Protocols*. 29–42. https://doi.org/10.1007/978-1-0716-0270-6_3 (2020).
38. Di Tommaso, P. et al. T-Coffee: A web server for the multiple sequence alignment of protein and RNA sequences using structural information and homology extension. *Nucleic Acids Res.* **39**, W13–W17 (2011).
39. Gouet, P., Robert, X. & Courcelle, E. ESPript/ENDscript: extracting and rendering sequence and 3D information from atomic structures of proteins. *Nucleic Acids Res.* **31**, 3320–3323 (2003).
40. da Guerra, J. V. pyKVFinder: an efficient and integrable Python package for biomolecular cavity detection and characterization in data science. *BMC Bioinform.* **22**, 607 (2021).
41. Chen, X. et al. Protenix-Advancing structure prediction through a comprehensive AlphaFold3 reproduction. *bioRxiv* 2021–2025 (2025).
42. Corley, N. et al. Accelerating biomolecular modeling with AtomWorks and RF3. *BioRxiv* (2025).
43. Berendsen, H. J. C., van der Spoel, D. & van Drunen R. GROMACS: A message-passing parallel molecular dynamics implementation. *Comput. Phys. Commun.* **91**, 43–56 (1995).
44. Brooks, B. R. et al. The biomolecular simulation program. *J. Comput. Chem. 30*. **CHARMM**, 1545–1614 (2009).
45. Kim, S. et al. CHARMM-GUI ligand reader and modeler for CHARMM force field generation of small molecules. *J. Comput. Chem.* **38**, 1879–1886 (2017).
46. Huang, J. & MacKerell, A. D. Jr CHARMM36 all-atom additive protein force field: Validation based on comparison to NMR data. *J. Comput. Chem.* **34**, 2135–2145 (2013).
47. Mark, P. & Nilsson, L. Structure and dynamics of the TIP3P, SPC, and SPC/E water models at 298 K. *J. Phys. Chem. A*. **105**, 9954–9960 (2001).
48. Cox, J. & Mann, M. MaxQuant enables high peptide identification rates, individualized p.p.b.-range mass accuracies and proteome-wide protein quantification. *Nat. Biotechnol.* **26**, 1367–1372 (2008).
49. Sánchez-Carbente, M. D. R. et al. The first description of a hormone-sensitive lipase from a basidiomycete: Structural insights and biochemical characterization revealed Bjerkandera adusta BaEstB as a novel esterase. *Microbiologyopen* **6**, (2017).
50. Gupta, R. S. The phylogeny of proteobacteria: relationships to other eubacterial phyla and eukaryotes. *FEMS Microbiol. Rev.* **24**, 367–402 (2000).
51. Zheng, Q. et al. An α/β-hydrolase fold protein in the biosynthesis of thiostrepton exhibits a dual activity for endopeptidyl hydrolysis and epoxide ring opening/macrocyclization. *Proc. Natl. Acad. Sci.* **113**, 14318–14323 (2016).
52. De Jaco, A., Comoletti, D., Dubi, N., Camp, S. & Taylor, P. Processing of cholinesterase-like α/β-hydrolase fold proteins: alterations associated with congenital disorders. *Protein Pept. Lett.* **19**, 173–179 (2012).
53. Bauer, T. L., Buchholz, P. C. F. & Pleiss, J. The modular structure of α/β-hydrolases. *FEBS J.* **287**, 1035–1053 (2020).

54. Mindrebo, J. T., Nartey, C. M., Seto, Y., Burkart, M. D. & Noel, J. P. Unveiling the functional diversity of the alpha/beta hydrolase superfamily in the plant kingdom. *Curr. Opin. Struct. Biol.* **41**, 233–246 (2016).
55. Perez-Garcia, P. et al. An archaeal lid-containing feruloyl esterase degrades polyethylene terephthalate. *Commun Chem* **6**, (2023).
56. Levisson, M., van der Oost, J. & Kengen, S. W. M. Characterization and structural modeling of a new type of thermostable esterase from Thermotoga maritima. *FEBS J.* **274**, 2832–2842 (2007).
57. Bornscheuer, U. T. Microbial carboxyl esterases: classification, properties and application in biocatalysis. *FEMS Microbiol. Rev.* **26**, 73–81 (2002).
58. Blodgett, J. A., Zhang, J. K., Yu, X. & Metcalf, W. W. Conserved biosynthetic pathways for phosalacine, bialaphos and newly discovered phosphonic acid natural products. *J. Antibiot.* **69**, 15–25 (2016).
59. Horsman, M. E., Hari, T. P. A. & Boddy, C. N. Polyketide synthase and non-ribosomal peptide synthetase thioesterase selectivity: Logic gate or a victim of fate? *Nat. Prod. Rep.* **33**, 183–202 (2016).
60. Ansari, M. Z., Yadav, G., Gokhale, R. S. & Mohanty, D. NRPS-PKS: A knowledge-based resource for analysis of NRPS-PKS megasynthases. *Nucleic Acids Res.* **32**, W405–W413 (2004).
61. Patel, K. D. et al. The structure of the monobactam-producing thioesterase domain of SulM forms a unique complex with the upstream carrier protein domain[Formula presented]. *Journal Biol. Chemistry* **300**, (2024).
62. Liu, Y., Zheng, T. & Bruner, S. D. Structural basis for phosphopantetheinyl carrier domain interactions in the terminal module of nonribosomal peptide synthetases. *Chem. Biol.* **18**, 1482–1488 (2011).
63. Sarkar, J., Dutta, A., Pal Chowdhury, P., Chakraborty, J. & Dutta, T. K. Characterization of a novel family VIII esterase EstM2 from soil metagenome capable of hydrolyzing estrogenic phthalates. *Microb. Cell. Fact.* **19**, 77 (2020).
64. Brault, G., Shareck, F., Hurtubise, Y., Lépine, F. & Doucet, N. Isolation and characterization of EstC, a new cold-active esterase from Streptomyces coelicolor A3 (2). *PLoS One*. **7**, e32041 (2012).
65. Suplatov, D. A., Besenmatter, W., Švedas, V. K. & Svendsen, A. Bioinformatic analysis of alpha/beta-hydrolase fold enzymes reveals subfamily-specific positions responsible for discrimination of amidase and lipase activities. *Protein Eng. Des. Selection*. **25**, 689–697 (2012).
66. Cantu, D. C., Chen, Y., Reilly, P. J. & Thioesterases A new perspective based on their primary and tertiary structures. *Protein Sci.* **19**, 1281–1295 (2010).
67. Caswell, B. T. et al. Thioesterase enzyme families: Functions, structures, and mechanisms. *Protein Sci.* **31**, 652–676 (2022).
68. Zheng, X. et al. Crystal Structure of a Novel Esterase Rv0045c from Mycobacterium tuberculosis. *PLoS One*. **6**, e20506 (2011).
69. Goldstone, D. C. et al. Structural and functional characterization of a promiscuous feruloyl esterase (Est1E) from the rumen bacterium Butyrivibrio proteoclasticus. *Proteins Struct. Funct. Bioinform.* **78**, 1457–1469 (2010).
70. Nardini, M. & Dijkstra, B. W. α/β Hydrolase fold enzymes: the family keeps growing. *Curr. Opin. Struct. Biol.* **9**, 732–737 (1999).
71. Wu, H. et al. Recycling of overactivated acyls by a type II thioesterase during calcimycin biosynthesis in Streptomyces chartreusis NRRL 3882. *Appl Environ. Microbiol* **84**, (2018).
72. Little, R. F. & Hertweck, C. Chain release mechanisms in polyketide and non-ribosomal peptide biosynthesis. *Nat. Prod. Rep.* **39**, 163–205 (2022).
73. Akey, D. L. et al. Structural basis for macrolactonization by the pikromycin thioesterase. *Nat. Chem. Biol.* **2**, 537–542 (2006).
74. Wang, W. G. et al. Molecular basis for the biosynthesis of an unusual chain-fused polyketide, Gregatin A. *J. Am. Chem. Soc.* **142**, 8464–8472 (2020).
75. Koglin, A. et al. Structural basis for the selectivity of the external thioesterase of the surfactin synthetase. *Nature* **454**, 907–911 (2008).
76. Frueh, D. P. et al. Dynamic thiolation–thioesterase structure of a non-ribosomal peptide synthetase. *Nature* **454**, 903–906 (2008).
77. Yang, W. et al. Structure-guided rational design of the Geobacillus thermoglucosidasius feruloyl esterase GthFAE to improve its thermostability. *Biochem. Biophys. Res. Commun.* **600**, 117–122 (2022).
78. Kasmaei, K. M. et al. Crystal structure of the feruloyl esterase from Lentilactobacillus buchneri reveals a novel homodimeric state. *Front Microbiol* **13**, (2022).
79. Omori, K. K. et al. The structure of a Lactobacillus helveticus chlorogenic acid esterase and the dynamics of its insertion domain provide insights into substrate binding. *FEBS Lett.* **597**, 2946–2962 (2023).
80. Lai, K. K. et al. An inserted α/β subdomain shapes the catalytic pocket of *Lactobacillus johnsonii* cinnamoyl esterase. *PLoS One*. **6**, 1–13 (2011).
81. Jeon, S. et al. Feruloyl Esterase (LaFae) from *Lactobacillus acidophilus*: Structural insights and functional characterization for application in ferulic acid production. *Int J. Mol. Sci* **24**, (2023).
82. Gao, D. W. et al. A Polyketide cyclase that forms medium-ring lactones. *J. Am. Chem. Soc.* **143**, 80–84 (2021).

83. Fellner, M. et al. Biochemical and cellular characterization of the function of fluorophosphonate-binding hydrolase H (FphH) in *Staphylococcus aureus* support a role in bacterial stress response. *ACS Infect. Dis.* **9**, 2119–2132 (2023).
84. Erickson, E. et al. Sourcing thermotolerant poly(ethylene terephthalate) hydrolase scaffolds from natural diversity. *Nat Commun* **13**, (2022).
85. Pinotsis, N. et al. Discovery of a non-canonical prototype long-chain monoacylglycerol lipase through a structure-based endogenous reaction intermediate complex. *Nat Commun* **14**, (2023).
86. Aschauer, P., Zimmermann, R., Breinbauer, R., Pavkov-Keller, T. & Oberer, M. The crystal structure of monoacylglycerol lipase from M. tuberculosis reveals the basis for specific inhibition. *Sci Rep* **8**, (2018).

Publisher's note Springer Nature remains neutral with regard to jurisdictional claims in published maps and institutional affiliations.

Authors and Affiliations

Pravin Kumran Nyanasegran[1] · Jia Rong Tey[1] · Anis Nadyra Zifruddin[1] · JiaXian Ong[1] · Sheila Nathan[2] · Glyn R. Hemsworth[3] · Mohd Firdaus-Raih[1,2,4] · Nor Azlan Nor Muhammad[1,4] · Chyan Leong Ng[1,4]

✉ Chyan Leong Ng
clng@ukm.edu.my

[1] Institute of Systems Biology, Universiti Kebangsaan Malaysia, Bangi 43600 UKM, Selangor, Malaysia

[2] Faculty of Science and Technology, Universiti Kebangsaan Malaysia, UKM Bangi, Selangor 43600, Malaysia

[3] Astbury Centre for Structural Molecular Biology, School of Molecular and Cellular Biology, Faculty of Biological Sciences, University of Leeds, Leeds LS2 9JT, UK

[4] Structural Biology and Protein Engineering Research Group, Universiti Kebangsaan Malaysia, Bangi 43600 UKM, Selangor, Malaysia